



13<sup>th</sup> World Conference on Earthquake Engineering  
Vancouver, B.C., Canada  
August 1-6, 2004  
Paper No. 479

## **FAULT INDUCED PERMANENT GROUND DEFORMATIONS — SIMULATIONS AND EXPERIMENTAL VERIFICATION**

**Jörgen JOHANSSON<sup>1</sup> and Kazuo KONAGAI<sup>2</sup>**

### **SUMMARY**

There are very few building codes in the world containing any type provisions for reducing the risks related to fault induced deformations. This may be due to the infrequent occurrence of fault surface ruptures, the great difficulty in preventing damage to infrastructure and buildings affected by the ruptures and also the difficult task of estimating the related permanent deformations due to many unknown factors such as possible fault location, geometry and motion; and mechanical properties of the soil deposit. To provide results in the form of possible extent and probabilities of deformation along these fault lines, much research is needed. The results from the dry and wet fault surface rupture 1-g model experiments are presented. A new computational code is introduced and simulation results are compared with the experimental results. The experiments show how the deformations and loads change substantially when water is present in a soil deposit as often is the case in nature. The code is verified for practical earthquake engineering purposes such as computing fault induced permanent deformations.

### **INTRODUCTION**

The 1999 earthquakes in Taiwan and Turkey have shown how great a risk fault ruptures is to human lives, buildings and infrastructure. Even though fault surface rupturing is not a new problem, there are very few building codes in the world containing any type provisions for reducing the risks. This may be due to the infrequent occurrence of fault surface ruptures, the great difficulty in preventing damage to infrastructure and buildings affected by the ruptures and also the difficult task of estimating the related permanent deformations due to many unknown factors such as possible fault location, geometry and motion; and mechanical properties of the soil deposit.

In California, United States; New Zealand; and also in Taiwan, after the 1999 earthquake, so called fault zoning acts have been established. A fault zoning act prevents construction within a certain distance of the known fault line and may be one way of reducing the risks for new buildings and infrastructure, but for structure already built along a fault line other remedial measures are needed, further more the fault zoning

---

<sup>1</sup>Research Associate, Earthquake Engineering Laboratory, Institute of Industrial Science, University of Tokyo, Japan

<sup>2</sup>Professor, Ditto

act does not say anything about the possible extent of deformations and/or the probability of occurrence of these deformations.

In highly populated countries such as Japan and other east and south-east Asian countries it is difficult to impose a fault-zoning act due to the lack of space. In these countries building code provisions based on engineering principles are needed as to allow for construction along fault-lines if certain design requirements are met. Such building code provisions would also be attractive for less populated countries, such as United States and New Zealand, as well, since it may allow for more economical construction.

Another issue is the difference between strike-slip and dip-slip faults. The deformations along a strike-slip seem to be concentrated in a narrower zone along the fault line whereas the deformations along a dip-slip fault may affect areas further away from the fault line [1]. In Japan there are some 90 dip-slip fault systems with several faults in each system and with a lot of buildings and infrastructure along them.

To provide results in the form of possible extent and probabilities of deformation along these fault lines, much research is needed. Previous research have mostly focused on dry cohesion-less [2] or clay materials in 1g- [3] and centrifuge tests [4].

The experiments described within here show how the deformations and loads change substantially when water is present in a soil deposit as often is the case in nature.

In combination with experimental findings a numerical tool can also give new insights. The authors [5] have developed numerical tool, which will be used for simulations of fault induced large soil movements to estimate the possible deformations that structures in and on top of soil deposit will undergo taking into account pore pressure effects. Simulation results are promisingly similar to the experimental findings.

## **EXPERIMENT SETUP AND PREPARATION**

To study in detail the effects on the deformation buildup due to a dip-slip fault when pore water is present in a soil, a new model experimental box has been designed and constructed as part of larger project involving fault surface ruptures. As can be seen in Figure 1 the box allows only for axi-symmetric fault experiment which is different from the more common 2-D plane strain experiments performed by other researchers. The box was designed with a round piston to simplify the construction of the water-proof box. A prototype structure is not considered rather these experiments will serve as a verification basis for numerical tools in which the experiment could be simulated with an axi-symmetric or 3-D model; or approximately simulated with a 2-D plain strain model. Nevertheless the experiment show many interesting features, which are discussed below.

The box in figure 1(a) measures 1.2 by 1.2 meters in plan and is 60 cm deep. In the bottom of the box and on top of the piston 6 pore pressure meters were installed as shown in figure 1(b). The 40 cm diameter piston, attached to a 300 kN hydraulic actuator, see figure 2(a), was lifted/pushed up through the soil to model a fault offset and induce the subsequent fault surface rupture.

In all experiments the piston displacement (vertical) was given as step function with smooth transition from zero to a maximum velocity of 6.5 cm/s and then a smooth transition to zero velocity resulting in a total uplift of 9.4 cm as shown by figure 2 .

Toyoura sand with a mean diameter,  $D_{50}$ , of 0.2 mm was air-pluviated into the box to assure repeatability and homogeneity with a pluviator with a wedge-shaped section and a box-wide slit opening of 0.8 mm. The pluviator moved back and fourth along the box at a fixed height. The sand fall height varied between 0.8 and 1.2 meters causing the void ratio to vary a few percent from the bottom to the top of the sand. Table 1 gives the average void ratios, a void ratio of 0.68 corresponds a density of 1580 kg/m<sup>3</sup>. To even out

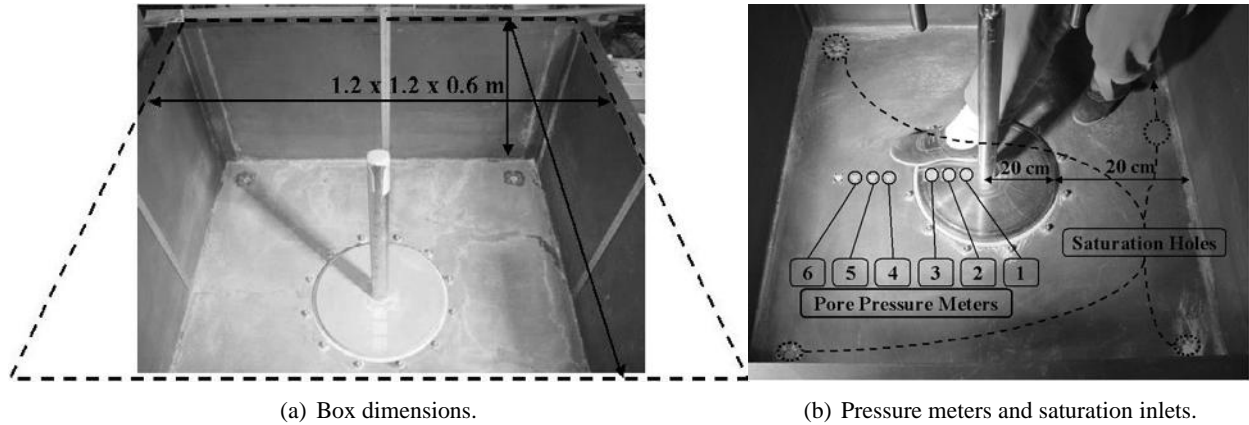


Figure 1: View inside the experiment box.

the sand thickness differences during the pluviation procedure, scraping was *not* used rather sand was only allowed to exit from the pluviator over areas of lower thickness. To be able to see the induced deformation the sand deposit was inter-layered with thin (3-5 mm) horizontal layers of colored Toyoura sand every 5 cm (see figure 4.) The total height of the sand was approximately 40 cm.

Three out of the total five experiments were saturated with regular tap water from an elevated water tank with 4 equal long hoses connected close to the corners at the bottom of the box. The saturation time varied between 15 and 20 hours depending on the amount of water in and the elevation of the tank. The elevation was regulated with a small crane at intervals to keep the water inflow approximately constant. An average saturation degree,  $S$ , of 80% was estimated by computing the voids volume and the water volume in the box. (The two dry experiments were saturated after the experiment to allow for sectioning.) The experimental parameters are summarized in table 1.

**Table 1: experiment parameters**

Experiment	1, dry	2, wet	3, dry	4, wet	5, wet
Density, $\rho$ [ $\text{Mg}/\text{m}^3$ ]	1.61	1.62	1.58	1.58	1.58
Avg. void ratio, $e$	0.65	0.63	0.68	0.68	0.68
Sat. deg., $S$ [%]	n/a	78	n/a	81	76

## EXPERIMENT RESULTS

Several different measurements were performed during and after the experiments. They include actuator load and displacement, pore pressures, surface displacements, wave speeds, sand densities, water contents, etc. Below a few selected data are given and analyzed. To remove higher frequency noise, a square or cosine window of varying length was convoluted with the raw data.

### Piston pressure versus displacement

Figure 3(a) shows the corrected actuator load normalized with the piston area ( $0.13 \text{ m}^2$ ) plotted versus the piston displacement. The pressure-displacement curves show an initial sudden peak and drop during the 1st mm displacement and then the pressure increases to reach a second peak at displacements of about 5

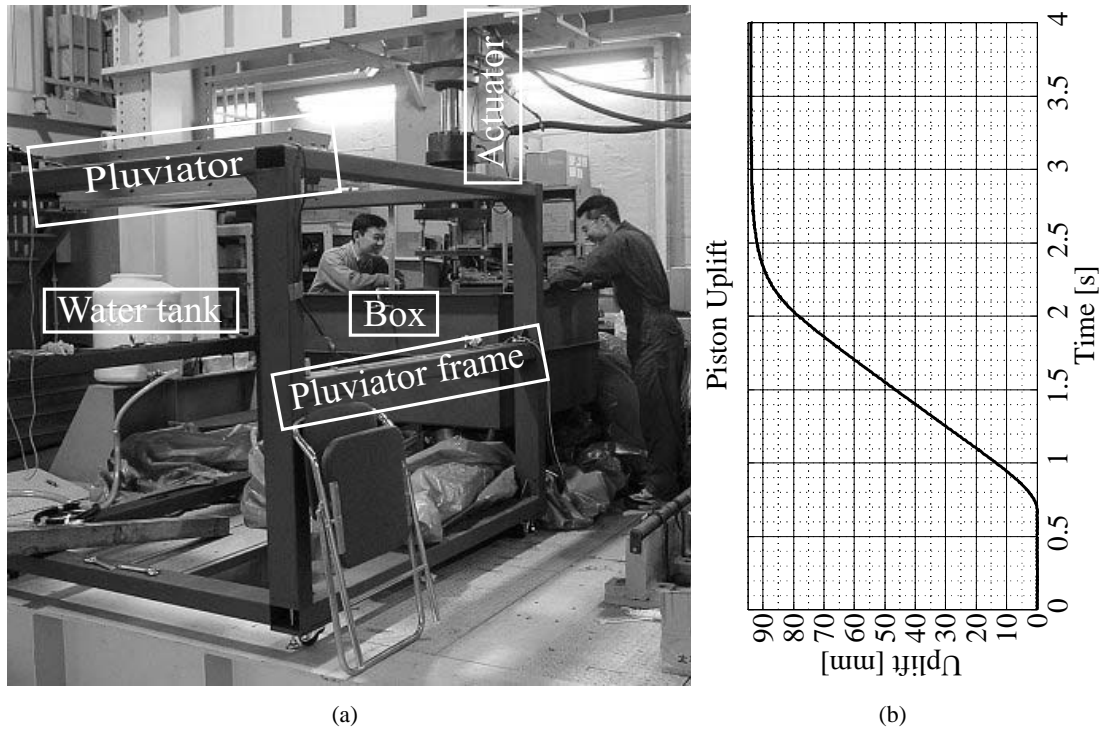


Figure 2: Experiment setup and piston uplift .

mm and 20-30 mm for the dry and wet experiments, respectively. The initial peak is an artifact due to a viscous stick-slip behavior of the actuator piston system, which is primarily caused by the Teflon fitting ring between the piston and the outer fixed cylinder. Several piston uplifts without any sand were performed and the ring-marked curve in figure 3(a) is an average with an initial peak of some 15 kPa and then empty piston resistance drops off to a level of about 12 kPa. The peak-displacement for the empty piston uplift varies and furthermore it is impossible to separate the response of the piston and the soil on top of it during the real experiments, thus the experimental data was corrected only by subtracting a value of 12.5 kPa from all data points.

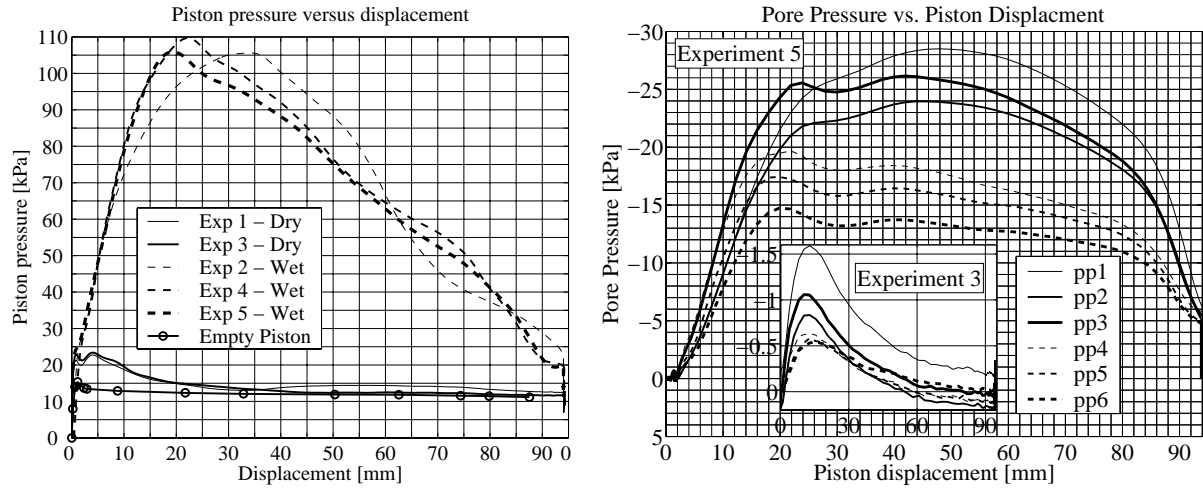
At the end of the uplift (at 94mm) all curves seem to converge to a pressure of about 12 kPa which corresponds to the weight of the piston itself and the truncated cone of soil on top of it. The self-weight of the piston itself corresponds to a 8.7 kPa pressure.

Figure 3(a) clearly shows the difference in piston pressure level between a dry and wet experiment and also how the peak piston pressure occurs at a larger displacement for the wet sand. For experiment 5 the second piston pressure peak coincides with the pore pressure peak for a piston uplift of 20 mm.

### Pore pressure

Figure 3(b) shows the pore pressures for the 6 pressure meters for experiments 3 (inset) and 5. (The pore pressure meters were set to zero before the experiment as to only measure excessive pressures built up during the experiment). In the dry experiment 3 the pore air pressure was measured and a maximum suction of 1.6 kPa was observed at pore pressure meter 1 (pp1). For the wet experiment 5 the maximum negative pore pressure was 28 kPa. As a reference the at rest static dry soil pressure is about 6 kPa (compressive).

The pressure peaks occur first at pressure meters closer to the piston edge, i.e. closer to the rupture zone and then at the pressure meters away from the rupture, either toward the middle of the piston or toward side of



(a) Piston Pressure versus displacement for all experiments. (b) Pore pressure versus piston displacement for exp. 3 (inset) and 5.

Figure 3: Piston pressure and pore pressures.

the box, for both dry and wet cases. The radial configuration of the experiment should cause magnification of the pressures closer to the piston center and this is confirmed by the higher negative pressures measured at pp1.

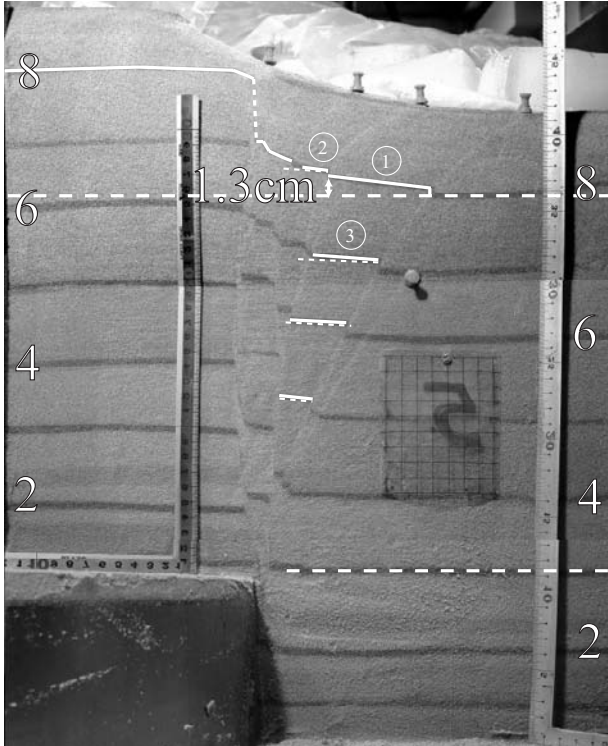
In the curves for pore pressure meters 1-6 for the wet experiment 5 there are two peaks, one at around 20 mm and one at between 40-45 mm displacement, which seem to correlate with the offsets in the white solid line in the section figure 4(b). The solid line is smoothly bent upward some 20 mm until it reaches a localization band and then it reaches a second localization band with a total offset of some 50 mm vertical from the originally horizontal line (dashed line in the figure.)

### Sections

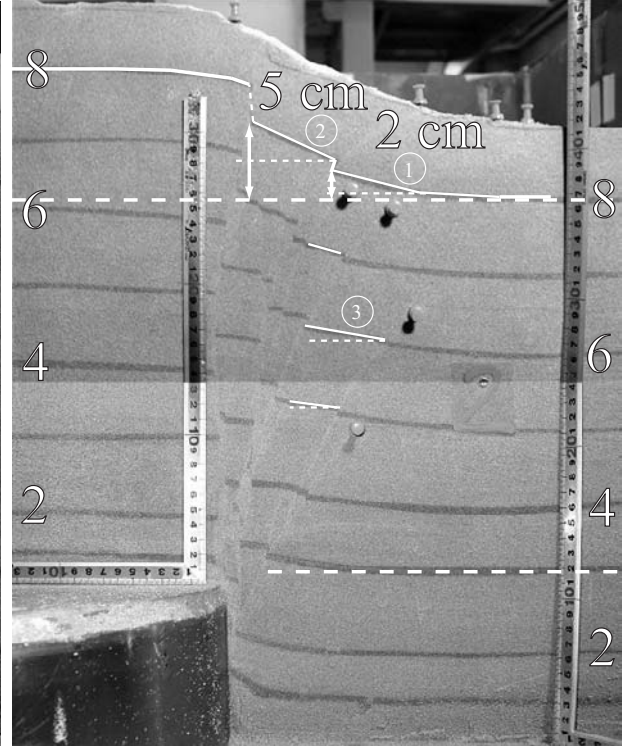
After the experiments the box was drained and the moist sand could be sectioned to study the deformations built up in the sand. For each experiment several sections were carefully cut, brushed and water-sprayed to obtain smooth surfaces for taking photos. Two sections from the dry experiment 3 and the wet experiment 5 are shown in figure 4. The soil deformation has localized into several about 2 to 3 mm wide bands and offset the dark horizontal lines. The shear-band or localization bands are readily seen as brighter lines crossing through darker less deformed zones. (When spraying water on the section before taking the photos, the localized bands, having a higher void ratio due to dilation during the experiments, dries out faster and leave dry bright lines in the darker moist surrounding soil.)

The sequence of the localization is from right to left i.e. the shear-band farthest away from the piston occurs first and the mainly vertical shear-band occurs last as others also reported [4, 6].

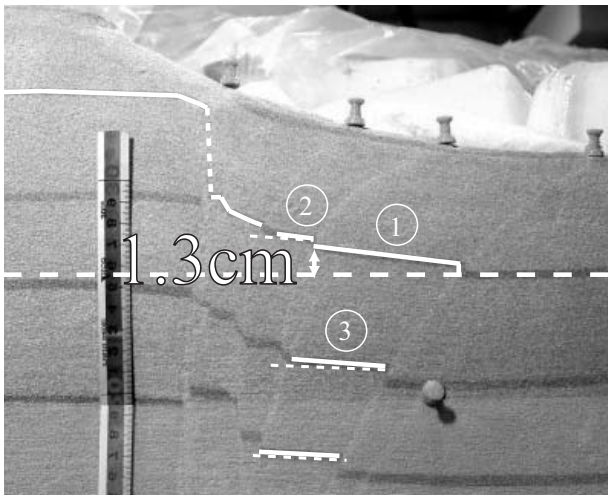
In the saturated case soil further away from the localization band is deformed, indicating that a larger part of the soil deformed before the deformation localization occurred. The horizontal white dashed lines are added as guides to the eye to see the upward bending of the soil when approaching the rupture. The observed negative pore water pressure (see figure 3) increases the effective stresses, thus increasing the failure strength of the soil, which then behaves elastically during a larger deformation than in the dry sand experiments. The inclinations of the numbered lines in figure 4 are given in table 2. The inclination is generally larger for the wet experiments.



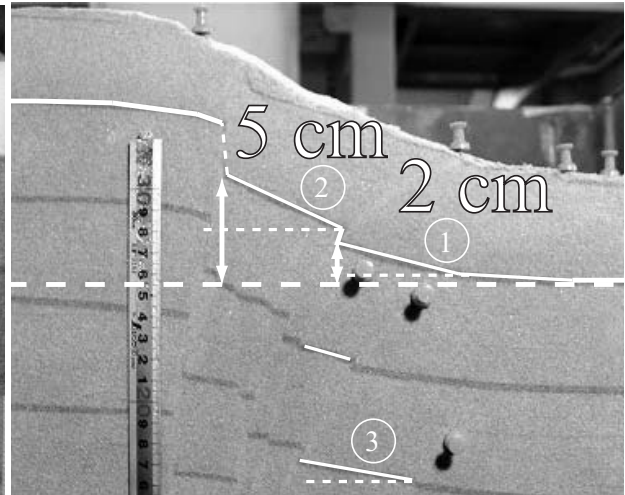
(a) Experiment 3 - dry



(b) Experiment 5 - wet



(c) Exp. 3 enlargement of upper part.



(d) Exp. 5 enlargement of upper part.

Figure 4: Section cut from experiment 3 (dry) and 5 (wet).

## NUMERICAL SIMULATIONS

Modelling of fault rupture induced deformations in overlying soil deposits is a difficult problem, whether experimentally or numerically. To take into account the scale of the problem either centrifuge model experiments or large scale numerical simulations could be used, both with their advantages and disadvantages.

**Table 2: Line inclinations.**

Experiment	1, dry	3, dry	4, wet	5, wet
Inclination of line 1 [%]	3.1	12	31	26
Inclination of line 2 [%]	11	12	31	46
Inclination of line 3 [%]	6.1	7.6	24	17

Centrifuge experiments involves many difficult task, such as selecting a prototype model, select the most important parameters to model taking into account the laws of similitude. Two difficulties with modelling saturated soils are the selection of an appropriate fluid with desired seepage parameters and choosing the soil's grain size.

Here we take another approach and try to use a numerical tool. Large scale numerical simulations may be a disputable area of research within earthquake engineering considering the many unknown or highly variable parameters needed as input data, but this argument may also be used in favor for numerical tools, since it is much easier to use a large set of model parameters in numerical tool than in a model experiment.

To comply with a minimal level trustworthiness a numerical tool should be at least verified with some type of experiments. A numerical tool developed by the authors is presented and the results are compared with the experimental findings above.

### **Numerical Tool**

The numerical tool, described in detail in [5], is based on the Material Point Method [7]. It is a fairly new method for solving problems in solid mechanics [8] and is an extension of a hydrodynamics code called FLIP [9] which, in turn, evolved from the Particle-in-Cell Method for fluid flow[10]. The tool can simply be described as 2-D plane strain explicit (time-stepping) finite element code where the Gauss (integration) points are free to move through a fixed mesh.

### **Solid-fluid interaction (SFI) formulation**

In addition to regular continuum analysis (drained/dry or undrained analysis) a coupled solid-fluid (SFI) also known as the u-w scheme described by Chan [11] has been adopted and adjusted for implementation in the Material Point Method. The u-w scheme assumes that the soil is fully saturated, Darcy's law is valid, soil grains are incompressible, and thermal changes are negligible. The governing equations also can be found in e.g. [12, 13] or chapter 2 in [14].

### **Soil model**

A hypo-plastic model [15] which is capable of modeling many of important characteristics of the soil describes the behavior of dense Toyoura sand used in the experiment. Table 3 gives simple descriptions of input parameters and values. A detailed description is given in [16].

The hypo-plastic model used suffers from the so called ratcheting problem which causes unrealistic volumetric straining for cyclic shearing. This problem have been treated by extending the model with a an elastic strain range [17] and with a material overlay model[18]. These additions to the model makes it more complicated and here only a large damping was applied as to reduce the intrinsic vibrations in the explicit solution procedure.

### **Problem setting and input parameters**

Figure 5 shows the problem setup with the material points (small circles) representing a soil deposit. The large circles and triangles represents boundaries. The boundary connected with a thin line is a simple moving boundary which is used to apply velocities to nearby nodes as to impose a deformation on the soil

**Table 3: Hypo-plastic parameters.**

Parameter	Value	Unit	Description
$\varphi_c$	30.0	[ $^\circ$ ]	Critical state friction angle
$h_s$	$2600 \cdot 10^6$	[Pa=N/m <sup>2</sup> ]	Stiffness parameter
$n$	0.27	[1]	Stiffness
$e_{d0}$	0.61	[1]	Minimum void ratio in stress free condition
$e_{c0}$	0.98	[1]	Critical state void ratio in stress free condition
$e_{i0}$	1.1	[1]	Maximum void ratio in stress free condition
$\alpha$	0.18	[1]	fitting parameter
$\beta$	1.1	[1]	fitting parameter
$e_{initial0}$	0.68	[1]	Initial void ratio (measured in experiment)
$E_{small}$	100	Pa	Very small confining pressure stiffness (for numerical stability)
$k$	$1.0 \cdot 10^{-3}$	m/s	Hydraulic Conductivity
$K_f$	$1.0 \cdot 10^8$	Pa	Fluid bulk modulus
$P_{ft}$	$-1.0 \cdot 10^5$	Pa	Cavitation Pressure of fluid (for water $-1.0 \cdot 10^5 \simeq -1$ ATM corresponds to absolute pressure of 0 Pa.)

**Table 4: Fault experiment simulation input parameters.**

Case	1	2	3	4	5
Computation type	Dry	Seepage	Undrained	Seepage	Seepage
Fluid bulk modulus, $K_f$ , Pa	n/a	$1.0 \cdot 10^7$	$1.0 \cdot 10^8$	$1.0 \cdot 10^8$	$1.0 \cdot 10^8$
Hydraulic Conductivity, $k$ , m/s	n/a	$1.0 \cdot 10^{-3}$	$1.0 \cdot 10^{-3}$	$1.0 \cdot 10^{-3}$	$1.0 \cdot 10^{-4}$

deposit. The squares numbered 1 and 2 shows the location for monitoring pore pressures. The mesh size was  $2.5 \times 2.5$  cm and the deposit was 0.6 m wide and 0.4 m tall (same size as in the experiment.) Table 4 shows the varying parameters for the five cases.

Since a 2-phase formulation was used to solve the fluid interaction equivalent bulk moduli, given in table 4, were selected to model the pore fluid mixture (air-water), based on an estimated saturation degree of about 80% and an average p-wave velocity of 140 m/s.

### Results and discussion

Figure 6(a) shows the piston pressure vs. piston displacement. As in the experiment the piston pressure is much larger for the wet cases (seepage/ undrained). The computed difference in piston pressure between dry and wet cases is about 2 times, which is less than the difference observed in the experiments (about 5 times) . One reason is the inability to model the shear band thickness appropriately in the present code (as in most other “regular” FEM codes.) The zigzag shape of the piston pressure-displacement curve is due to motion of the material point through mesh. These fluctuations can be reduced by increasing the number of integration points and reducing the element size. The star-marked curve shows the results from case 5 with 4x4 integration points in stead of 2x2.

Figure 6(b) shows the pore pressure measured at location 1 and 2 vs. piston displacement for cases 2-5. Seepage cases 2, 4 and 5 show similar behavior initially a small compression (positive values) and then for a piston displacement of 1.5 cm a peak pore pressure is reached of about -35kPa (suction) at location 1 and -15kPa at location 2 for Case 2 and similarly for Case 4 about -45kPa (suction) at location 1 and -17kPa at

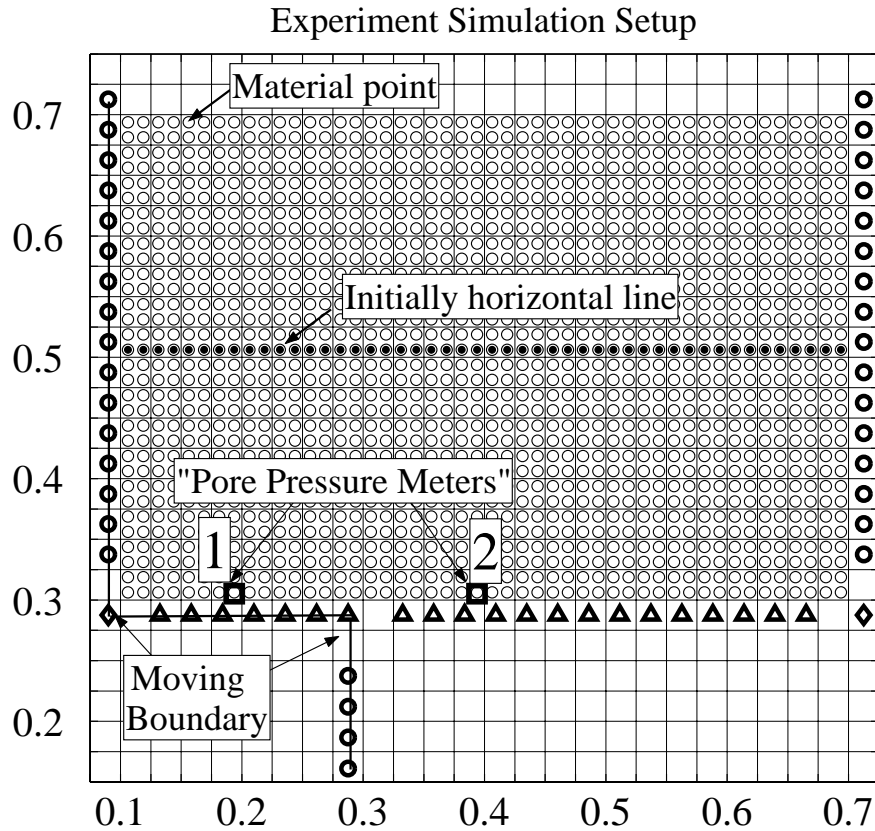


Figure 5: Problem setup. Units in meters.

location 2, while the pressures for Case 5 (with a lower hydraulic conductivity) the pressures magnitudes are larger and also here the fluctuations are less for Case 5 with 4x4 integration points. The undrained Case 3 shows a quite different pore pressure behavior. At location 1 a maximum compression of 170kPa at 1.5cm uplift and at location 2 a sucking pore pressure 50kPa are computed. In general the results for the seepage cases are in much better agreement with the experimentally observed values.

Figure 7 shows the maximum shear strains for the different cases at a piston uplift of 9.4 cm. (Compare with figure 4.) The undrained simulation (Case 3) has a much less clear shear band than other cases. The dry and seepage cases. After a piston uplift of about 2.3 cm (figures not shown here) the shear band for the seepage cases is slightly more vertical than for the dry case. (The undrained case show no clear shear band at all.) It seem to be necessary to allow for the fluid flow to take place to appropriately model the fault induce deformations in water saturated soil deposits.

When estimating fault induced effects on underground structures the permanent deformation of the soil is of interest and figure 8(a) compares the deformed shape obtained from the experiments and the simulations. The solid circles in figure 5 give the initial location of the horizontal line. For the wet cases, both for experiments and simulation, the affected zone is wider (soil deformation occurs further away from the piston edge) and the total uplift is larger.

The piston load-displacement results are damping dependent allowing only for relative comparison of the results. 8(b) shows the vertical and horizontal deformation of an initially horizontal line Case 1 without fluid, Case 3 undrained analysis, and Case 5-7 seepage formulation, all computed with same amount of damping. Material parameters are the same for all cases except for cases 6 and 7 where the damping was

reduced to one half and one tenth respectively.

The total uplift for the dry case is less than for the cases with fluid. In fact the vertical uplift of the horizontal line for the wet cases is larger than the uplift of the bottom boundary (representing the upward moving bed-rock). This can be explained by that the sheared part of the soil dilates and the pore fluid prevents the compression of the surrounding less sheared soil to compress so soil is pushed upward. For the dry case the soil that is not sheared can accommodate some of the volumetric increase in the shear zone, thus less vertical deformation is observed.

The deformation difference between Cases 5-7 are much smaller than the difference is between the dry Case 1, undrained Case 3 and seepage Case 5. This gives confidence in the computed permanent deformations are only slightly dependent on the amount of damping. Considering all the uncertainties in deciding real material parameters and not to mention the magnitude and velocity of displacement of the underlying bedrock, the difference in in computed deformations are of less importance.

Even though several things can be improved in present numerical scheme, for practical earthquake engineering purposes such as the application to fault induced permanent deformations the code suffice and can be considered verified.

## SUMMARY AND CONCLUSIONS

The results from the dry and wet fault surface rupture 1-g model experiments are presented. A new computational code is introduced and simulation results are compared with the experimental results.

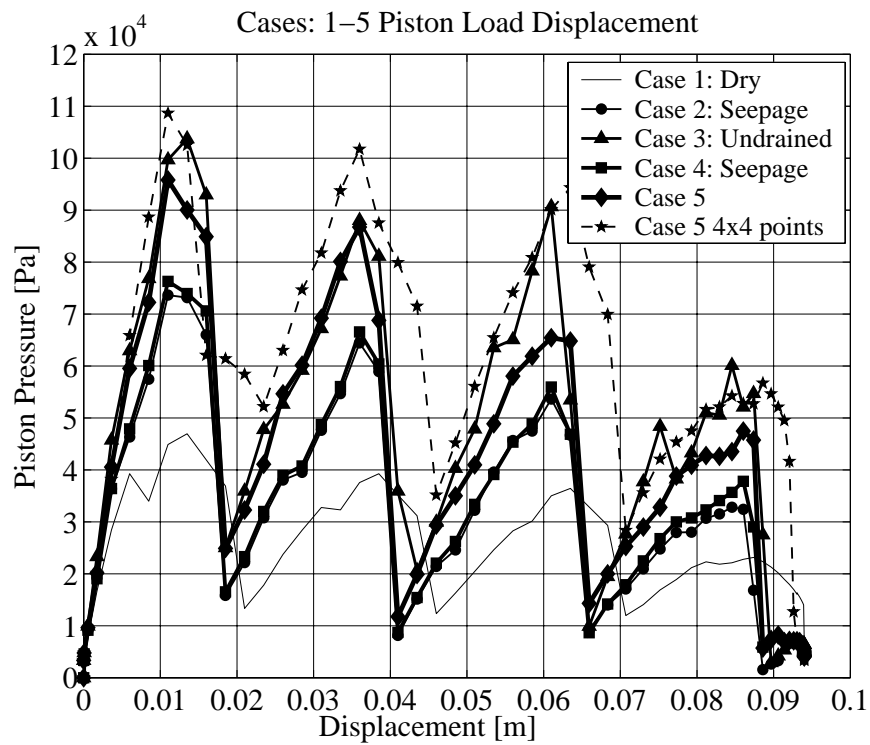
Important observations from the experiments are:

- The required actuator load (piston pressure) to cause the rupture is substantially (almost 5 times) larger for the wet soil.
- The deformations seem to localize at a later stage for the wet soil indicated by the piston pressure displacement curve and also observed in the sections where the initially horizontal lines are more inclined for the wet soil.
- The peaks in piston pressure and pore pressure are strongly correlated.

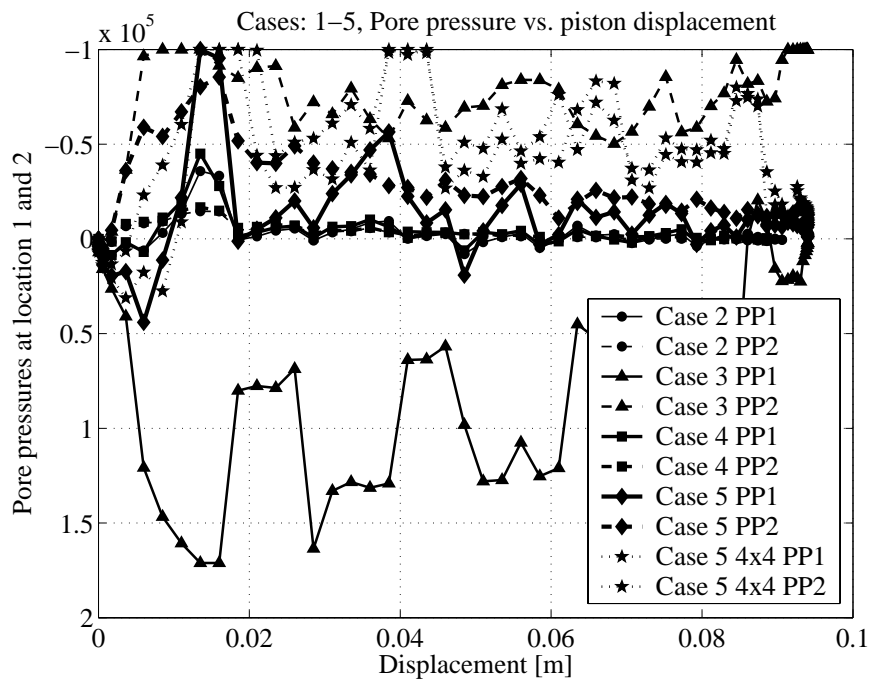
Important observations from the simulations are:

- It is necessary to take into account the fluid flow to appropriately model the wet experiments.
- The computed difference between dry and wet cases is about 2 times. One reason is the inability to model the shear band thickness appropriately.
- The observed pore pressure are of the same order as the ones observed in the experiment.
- The computed permanent deformations are only slight damping dependent.
- The code is verified for computing fault induced permanent deformations.

For the wet cases, both for experiments and simulation, the affected zone is wider (soil deformation occurs further away from the piston edge) and the total uplift is larger.



(a) Piston pressure vs. displacement



(b) Pore pressures vs. displacement. Observe the different scales.

Figure 6: Piston pressure and pore pressures for all cases.

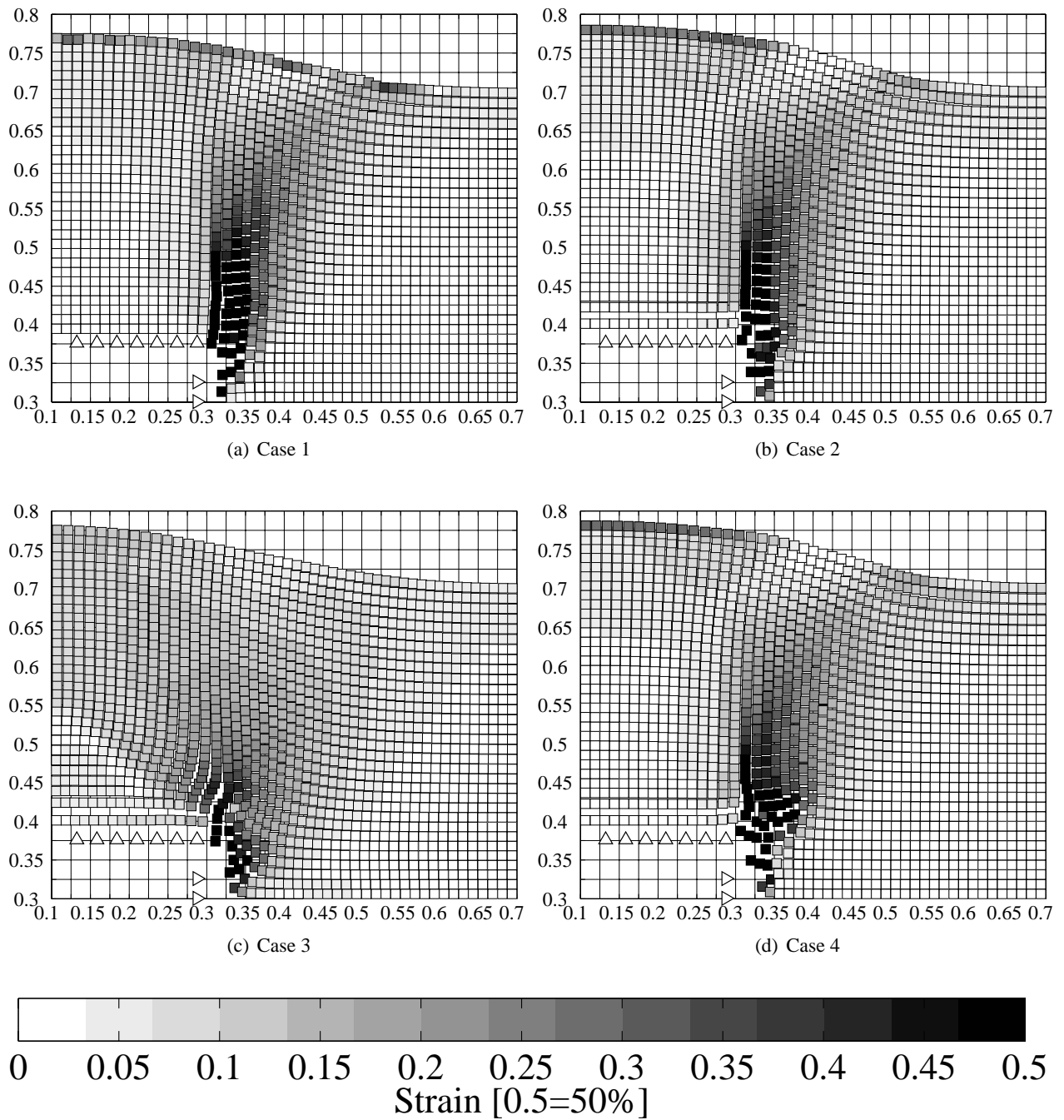


Figure 7: Maximum shear strains for all cases.

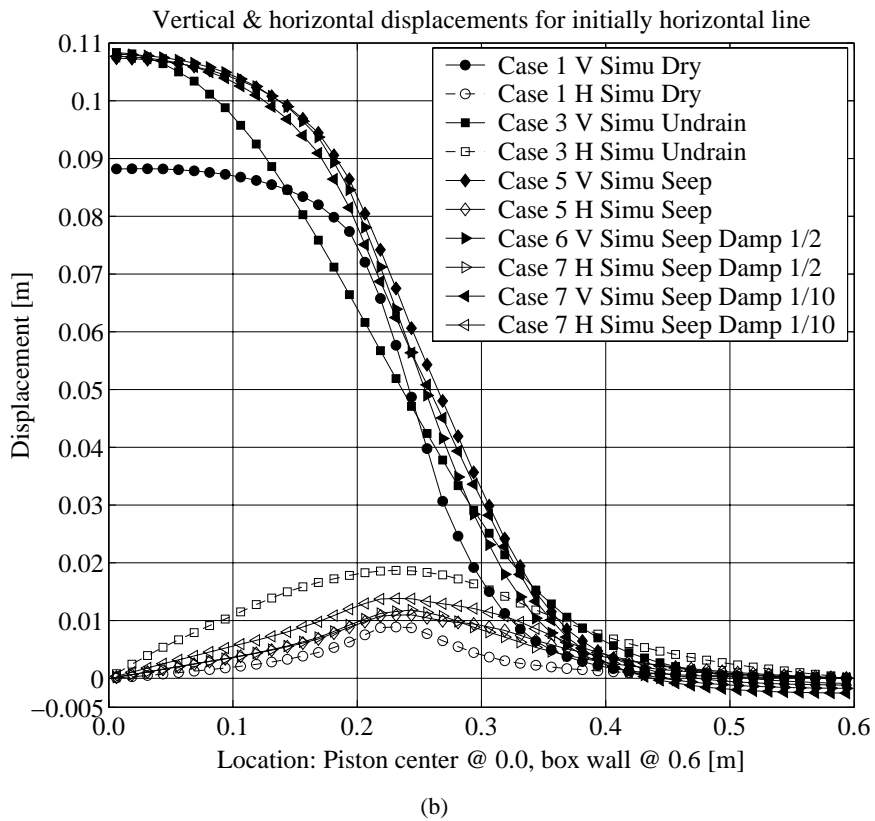
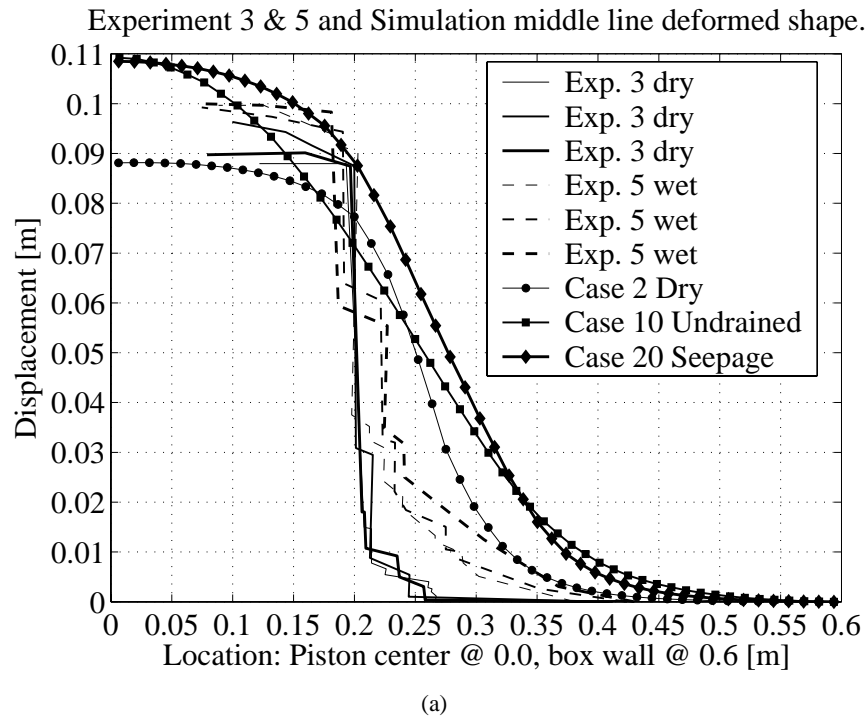


Figure 8: Deformation of initially horizontal lines.

## ACKNOWLEDGMENT

We would like to thank everyone who helped the first author while preparing for and performing the experiments. This research was supported by a part of the grant-in-aid No. 12355020 for scientific research (A) from the Japan Society for the Promotion of Science and is gratefully acknowledged. The first author also acknowledges the financial support in form a doctoral study scholarship by the Ministry of Education, Sports, and Culture of Japan.

## REFERENCES

### References

1. Mukoyama S. "Fault induced surface configuration features (in Japanese)." Mountain Geomorphology, Kokonshoin Press, 2000. 82–100.
2. Cole DAJ, Lade PV. "Influence zones in alluvium over dip-slip faults." Journal of Geotechnical Engineering 1984: 110(5): 597–615.
3. Bray JD, Seed RB, Cluff LS, Seed HB. "Earthquake fault rupture propagation through soil." Journal of Geotechnical Engineering 1990: 120(3): 543–580.
4. Stone KJL, Wood D. "Effects of dilatancy and particle size observed in model tests on sand." Soils and Foundations 1992: 32(4): 43–57.
5. Johansson J, Konagai K. "Modeling of large deformations of saturated soils during fault surface ruptures." Bulletin of earthquake resistant structure research center, Earthquake resistant structure research center, Institute of Industrial Science, University of Tokyo, 2003, 36. 17–34.
6. Lade PV, Cole DAJ. "Multiple failure surfaces over dip-slip faults." Journal of Geotechnical Engineering 1984: 110(5): 616–627.
7. Sulsky D, Chen Z, Schreyer HL. "A particle method for history-dependent materials." Computational Methods in Applied Mechanics and Engineering 1994: 118: 179–196.
8. Sulsky D, Zhou SJ, Schreyer HL. "Application of particle-in-cell method to solid mechanics." Computer Physics Communications 1995: 87: 236–252.
9. Burgess D, Sulsky D, Brackbill J. "Mass matrix formulation of the flip particle in cell method." Journal of Computational Physics 1992: 103: 1–15.
10. Harlow FH. "The particle-in-cell computing method for fluid dynamics in fundamental methods in hydrodynamics." Experimental Arithmetic, High-Speed Computations and Mathematics, Academic Press, 1964. 319–345.
11. Chan A, OO F, Wood MD. "A fully explicit u-w scheme for dynamic soil and pore fluid interaction." Cheung, Lee, Leung, editors, Asian Pacific Conference on Computational Mechanics. Balkema, Rotterdam, 1991, 881–887.
12. Zienkiewicz O, Chan A, Pastor M, Paul D, Shiomi T. "Static and dynamic behaviour of geomaterials - a rational approach to quantitative solutions, part i: Fully saturated problems." Proceedings of the Royal Society of London 1990: A429: 285–309.

13. Lewis R, Schrefler B. The finite element method in the static and dynamic deformation and consolidation porous media. West Sussex, England: John Wiley and Sons, 1998, 2 edition.
14. Zienkiewicz O, Chan A, Pastor M, Schrefler B, Shiomi T. Computational geomechanics with special reference to earthquake engineering. West Sussex, England: John Wiley and Sons, 1999.
15. Von Wolfersdorff PA. "A hypoplastic relation for granular materials with a predefined limit state surface." *Mech. Cohes.-Frict. Mater.* 1996: 1: 251–271.
16. Herle I, Gudehus G. "Determination of parameters of a hypoplastic constitutive model from properties of grain assemblies." *Mechanics of Cohesive-Frictional Materials* 1999: 4: 461–486.
17. Niemunis A, I H. "Hypoplastic model for cohesionless soils with elastic strain range." *Mechanics of Cohesive-Frictional Materials* 1997: 2: 279–299.
18. Niemunis A, Triantafyllidis T. "Liapunov instability of the hypoplastic model for soils." *Soil Dynamics and Earthquake Engineering* 2004: 24: 35–48.